

SI Appendix

Single-Molecule and -Particle Probing Crystal Edge/Corner as Highly Efficient Photocatalytic Sites on a Single TiO₂ Particle

Wei-Kang Wang,^{†,‡,#} Jie-Jie Chen,[†] Zai-Zhu Lou,[‡] Sooyeon Kim,[‡] Mamoru Fujitsuka,[‡]
Han-Qing Yu[†], and Tetsuro Majima[‡]

[†]Chinese Academy of Sciences Key Laboratory of Urban Pollutant Conversion,
Department of Applied Chemistry, University of Science & Technology of China,
Hefei, 230026, China

[‡]The Institute of Scientific and Industrial Research (SANKEN), Osaka University,
Mihogaoka 8-1, Ibaraki, Osaka, 567-0047, Japan

[#]Department of Chemistry, Tongji University, Shanghai, 200000, China

- Supplementary Discussion

Part S1. The detailed explanations for why the corner exhibited better electron transfer than the edge area.

- Supplementary Methods

Text S1. Chemicals and synthesis of anatase TiO₂ particles

Text S2. Characterization of anatase TiO₂ particles

Text S3. Computational methods

- Supplementary Figures

Fig. S1. XRD patterns (A) and SEM image (B) of anatase TiO₂ particles. The inset in (B) is a single anatase TiO₂ particle. TEM image (C) and high-resolution TEM image (D) of anatase TiO₂ particle. The inset in (D) is SAED pattern.

Fig. S2. XPS of anatase TiO₂ nanoparticles: Ti 2p (A), O 1s (B), F 1s (C), and C 1s (D).

Fig. S3. Phase-contrast microscope image (A) and the corresponding SEM image (B) for the anatase TiO₂ particle.

Fig. S4. Scheme showing several sites of a single anatase TiO₂ particle: surface S₁-S₄, edge E₀₀₁₋₁-E₀₀₁₋₄, edge E₁₀₁₋₁-E₁₀₁₋₄, and corner C₁-C₄.

Fig. S5. PL spectra at several sites on a single anatase TiO₂ particle: (A) surface S₁-S₄, (B) edge E₀₀₁₋₁-E₀₀₁₋₄, (C) edge E₁₀₁₋₁-E₁₀₁₋₄, and (D) corner C₁-C₄.

Fig. S6. PL decay profiles observed at several sites of a single anatase TiO₂ particle: (A) surface S₁-S₄, (B) edge E₀₀₁₋₁-E₀₀₁₋₄, (C) edge E₁₀₁₋₁-E₁₀₁₋₄, and (D) corner C₁-C₄.

Fig. S7. Emission decay profiles and intensity-weighted emission lifetimes measured with error bars at various areas from the middle (S_m), S, E₀₀₁, and E₁₀₁ to the corner (C) of an anatase TiO₂ particle. (A, B) for the particle in Fig. 2A, (C, D) for the particle in Fig. 3A, (E, F) for the particle in Fig. 3D.

Fig. S8. (A, D) PL lifetime images of a single anatase TiO₂ particle ($\lambda_{\text{ex}} = 405$ nm, a femtosecond pulsed laser) (intensity bar: 0-4.5 ns); (B, E) the corresponding PL spectra at several sites; (C, F) the corresponding PL decay profiles from the middle site to the corner site for a single anatase TiO₂ particle.

Fig. S9. (A, C) Phase-contrast microscope images (scale bar: 10 μm); (B, D) high-resolution SEM images for a single anatase TiO₂ particle for the measurement of PL decay profiles as shown in **Fig. S5**.

Fig. S10. PL (A, C) lifetime images of a single anatase TiO₂ particle ($\lambda_{\text{ex}} = 405$ nm, a femtosecond pulsed laser) (Intensity bar: 0-4.5 ns); (B, D) phase-contrast microscope images (scale bar: 10 μm).

Fig. S11. Fluorogenic probe reactions: (A) oxidation of amplex red, (D) reduction of resazurin under UV irradiation of TiO₂ aqueous suspension. Absorption spectral changes in the oxidation (B) and reduction (E). Fluorescence spectral changes in the oxidation (C) and reduction (F). $\lambda_{\text{ex}} = 532$ nm.

Fig. S12. Single-molecule fluorescence images on a single TiO₂ particle for the photocatalytic oxidation of amplex red (A) and reduction of resazurin (B) (scale bar: 1 μm).

Fig. S13. Single-molecule fluorescence images on a single TiO₂ particle for the photocatalytic oxidation of amplex red at times of 0 (A), 4.5 (B), and 48.0 s (C) and the photocatalytic reduction of resazurin at times of 0 (D), 18.5 (E), and 52.8 s (F). Scale bar, 1 μm.

- Supplementary Tables

Table S1. PL lifetimes at several sites of anatase TiO₂ particles (**Fig. 2A**)

Table S2. PL lifetimes at several sites of anatase TiO₂ particles (**Fig. 3A**)

Table S3. PL lifetimes at several sites of anatase TiO₂ particles (**Fig. 3D**)

Table S4. Calculated thermodynamic (Gibb's free energy change, ΔG) and kinetic properties (energy barrier, E_a) of the fluorogenic probe reactions on anatase TiO₂ (001) surface and (101) surface, and their crystal edge.

- Supplementary References

- Supplementary Movies

Movie S1. Single-molecule reaction on a single TiO₂ particle for the photocatalytic oxidation of amplex red

Movie S2. Single-molecule reaction on a single TiO₂ particle for the photocatalytic reduction of resazurin

Supplementary Discussion

Part S1. The detailed explanations for why the corner exhibited better electron transfer than the edge area.

The TiO₂ corner exhibits better electron transfer than the edges because of the following two reasons:

(1) Less coordination number

To combine with substrates, the surface atoms must have unsaturated coordination, and the coordination number may drastically affect the catalytic performance. Since corners of nanoparticles feature a lower coordination number than atoms on edges, the chemical environment of corners in multicomponent interfaces is different from that of the other parts to be used to tune the electronic structure and the catalytic performance. In general, a lower coordination number is related to a higher active center¹. For anatase TiO₂, the coordination number of Ti atom on (001) or (101) surface, on the edge, and at the corner is 5, 4, and 3, respectively^{2,3}. Thus, the corner is preferred to bind with the dye molecules, leading to the efficient electron transfer reactions.

(2) Greater localized electric field enhancement

The electron transfer also depends on the shape of the nanoparticles⁴. Considering corner sharpness, the calculations of the near-fields around nanoparticles show that surface charges are accumulated at sharp corners⁵. As a result of such an enhanced charge separation, the restoring force for electron oscillation is reduced. More importantly, the sharp corners on the nanoparticles provide a greater localized electric field enhancement than the rounded ones.

Therefore, the TiO₂ corners with less coordination number and greater localized electric field enhancement exhibited more efficient electron transfer than the edges.

Supplementary Methods

Text S1. Chemicals and synthesis of anatase TiO₂ particles

Briefly, 65 mg of TiOSO₄ was dissolved in 40 ml HF (120 mmol L⁻¹) solution in a 50 mL beaker. After 30-min stirring, the solution was transferred into a polytetrafluoroethylene (Teflon)-lined stainless autoclave with a total volume of 50 mL. The hydrothermal reaction was conducted at 180 °C for 12 h in an electric oven. The autoclave was cooled to room temperature after the growth process. The obtained samples were ultrasonically cleaned using ethanol and water in sequence. Before single-molecule and -particle measurements, anatase TiO₂ particles were treated with NaOH (0.1 M) to remove the adsorbed fluorine ions.

Text S2. Characterization of anatase TiO₂ particles

The power X-ray diffraction (XRD) pattern was obtained by a Rigaku diffractometer (Rint-2500, Rigaku, Co., Japan), using a Cu K α radiation source ($\lambda=1.541841$ Å) at a scan speed of 8 °/min. The morphology and microstructure of the TiO₂ nanostructures were imaged by a field-emission scanning electron microscope (SEM, JSM-6330FT, JEOL Inc., Japan). High-resolution transmission electron microscopy (HRTEM) images were obtained on a transmission electron microscope with an accelerating voltage of 300 kV (JEM 3000F, JEOL Inc., Japan).

Text S3. Computational methods

Model structure. On the basis of TiO₂ model used in ref. 6, the cluster model contains 33 Ti atoms and 64 O atoms in a supercell (39.00 × 3.78 × 28.00 Å) with both (001) surface and (101) surface, and their crystal edge of anatase TiO₂. The vacuum region between the neighboring unit cells is larger than 15.0 Å to neglect their neighboring interaction. The (001) faces shows two-fold coordinated oxygen (O-2c) between two penta-coordinated titanium atoms (Ti-5c), with Ti-O-Ti angles of 156°. ⁷ The (101) facet exhibits a sawtooth-like configuration with Ti-5c, Ti-6c, O-2c, and O-3c. The electronic structure and photocatalytic performance (thermodynamic and kinetic properties) of the crystal edge are compared with those of (001) and (101) facets.

Band alignment. The band alignment in Fig. 5c was determined according to the calculated DOS results as shown in Fig. 5b. Although the band gap is underestimated by theoretical calculations, density functional theory is formally exact for calculating the band gap center (BGC), denoted by E_{BGC} . ⁸ Then, the position of conduction band minimum (CBM) and valence band maximum (VBM) could be determined as follows,

$$E_{VBM} = E_{BGC} - 1/2E_g \quad (1)$$

$$E_{CBM} = E_{BGC} + 1/2E_g \quad (2)$$

where E_g is the energy gap from experimental measurement, i.e., 3.18 and 3.22 eV for TiO₂ (001) and (101) surfaces, respectively. ⁶ However, until now, the experimental E_g at crystal edge cannot be measured. Therefore, the average value (3.20 eV) of the (001) and (101) surfaces is temporarily used instead of this experimental value under the circumstances of (001) and (101) surfaces coexisting. Moreover, the work function Φ ,

defined as the minimum energy required for removing an electron from a material, affects the energy alignment in determining the valence- and conduction-band positions relative to the vacuum level.⁹ The calculated work function of the (001) and (101) facets obtained using slab models is 6.42 and 6.99 eV, respectively.⁶ Similarly, the work function at crystal edge was temporarily set as the average value (6.705 eV) of the (001) and (101) facets for the lack of the calculation methods for the edge position. Thus, the E_{BGC} relative to the vacuum level would be $E_{\text{BGC}}' = E_{\text{BGC}} - \Phi$. Then, the VBM and CBM could be aligned relative to the vacuum level.

Free energy calculations. In the photocatalytic process, the Gibbs free energy changes (ΔG) value of the fluorogenic probe reactions involving proton and hole (Table S2) should deduct the energy of electron-hole pair generation.¹⁰ The oxidation of amplex red could also be written as $\text{TiO}_2\text{-amplex red} + \text{H}_2\text{O} + 2\text{h}^+ \rightarrow \text{TiO}_2\text{-resorufin} + \text{CH}_3\text{COOH} + 2\text{H}^+$, and changed to $\text{TiO}_2\text{-amplex red} + \text{H}_2\text{O} + 2\text{h}^+ + 2\text{e}^- \rightarrow \text{TiO}_2\text{-resorufin} + \text{CH}_3\text{COOH} + 2\text{H}^+ + 2\text{e}^-$. Thus, the ΔG of the photocatalytic reaction occurring on valence band is shown as:

$$\Delta G = G(\text{TiO}_2\text{-resorufin}) + G(\text{H}^+ + \text{e}^-) - G(\text{TiO}_2\text{-amplex red}) - G(\text{h}^+ + \text{e}^-). \quad (\text{S1})$$

Using the standard hydrogen electrode (SHE) as the reference, $\text{H}^+ + \text{e}^- \rightarrow 1/2 \text{H}_2$ ($\text{pH} = 0$, $p = 1 \text{ bar}$, $T = 298.15 \text{ K}$), $\Delta G_{\text{H}} = 1/2G(\text{H}_2) - G(\text{H}^+ + \text{e}^-) = 0$, Eq (S1) can be rewritten as:

$$\Delta G = G(\text{TiO}_2\text{-resorufin}) + 1/2G(\text{H}_2) - G(\text{TiO}_2\text{-amplex red}) - |e|U \quad (\text{S2})$$

where U is the electropotential of a photogenerated hole with respect to SHE ($U = 0$, $\Delta G_{\text{H}} = 0$), and thus, $|e|U$ represents the extra energy required to generate the electron-

hole pair^{10,11} for the oxidation of amplex red.

For this cluster model of anatase TiO₂, no additional energy is needed for the oxidation of amplex red on (001) surface and at the crystal edge.

Supplementary Figures

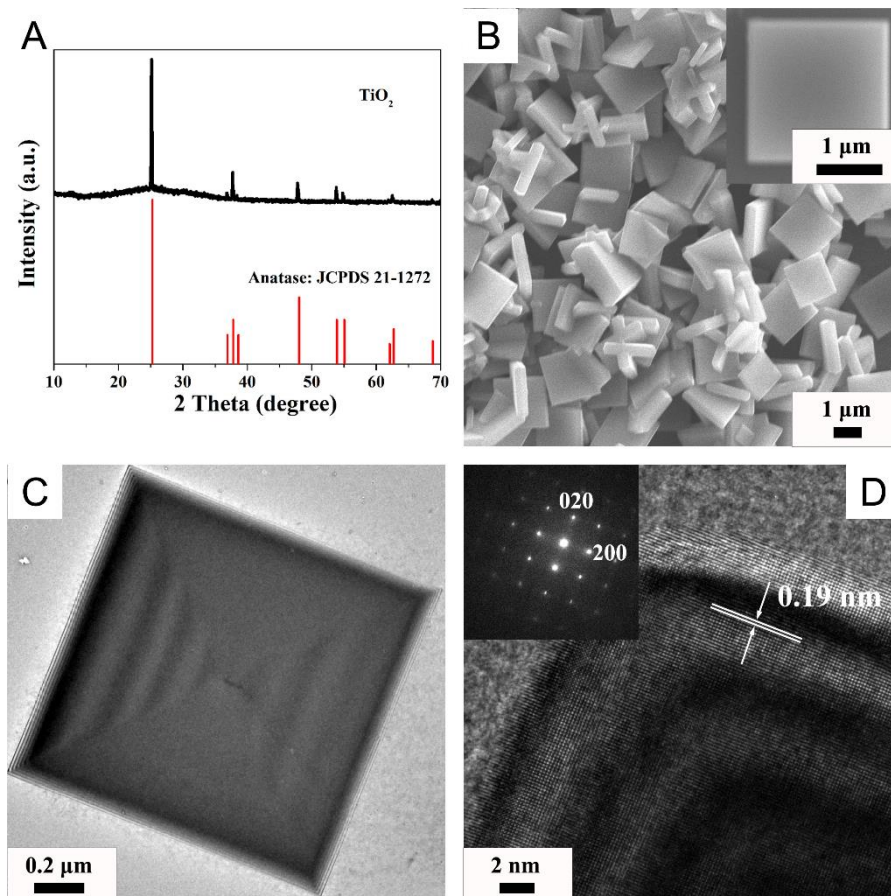


Fig. S1. XRD patterns (A) and SEM image (B) of anatase TiO₂ particles. The inset in (B) is a single anatase TiO₂ particle. TEM image (C) and high-resolution TEM image (D) of anatase TiO₂ particle. The inset in (D) is SAED pattern.

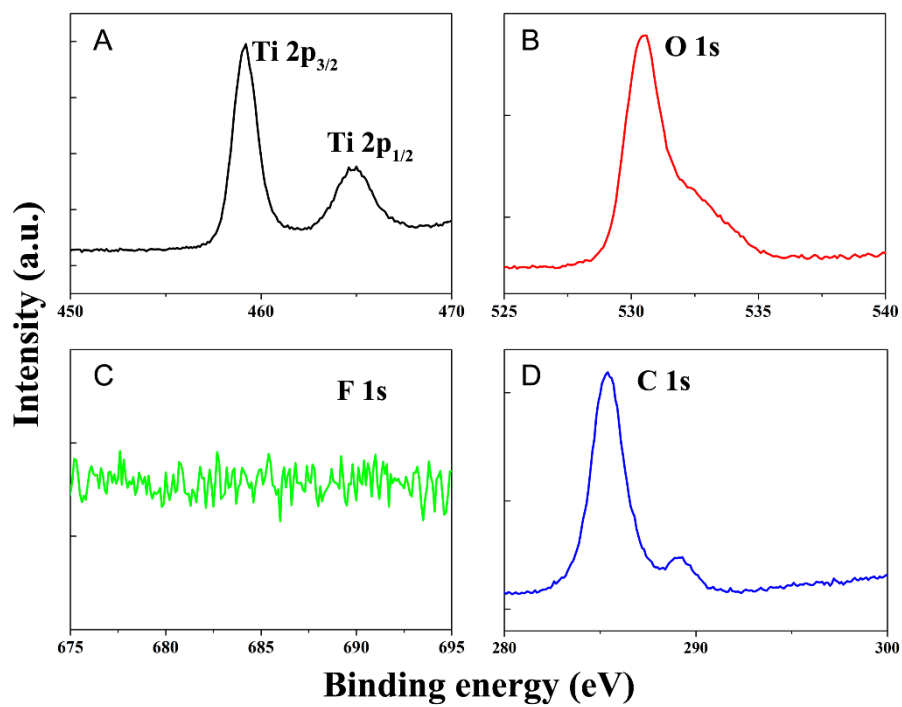


Fig. S2. XPS of anatase TiO₂ nanoparticles: Ti 2p (A), O 1s (B), F 1s (C), and C 1s (D).

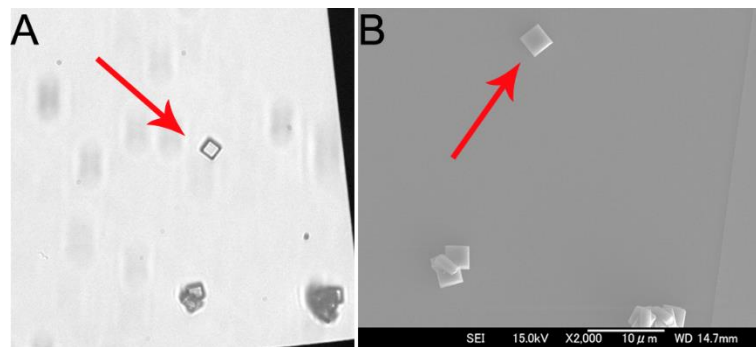


Fig. S3. Phase-contrast microscope image (A) and the corresponding SEM image (B) for the anatase TiO₂ particle.

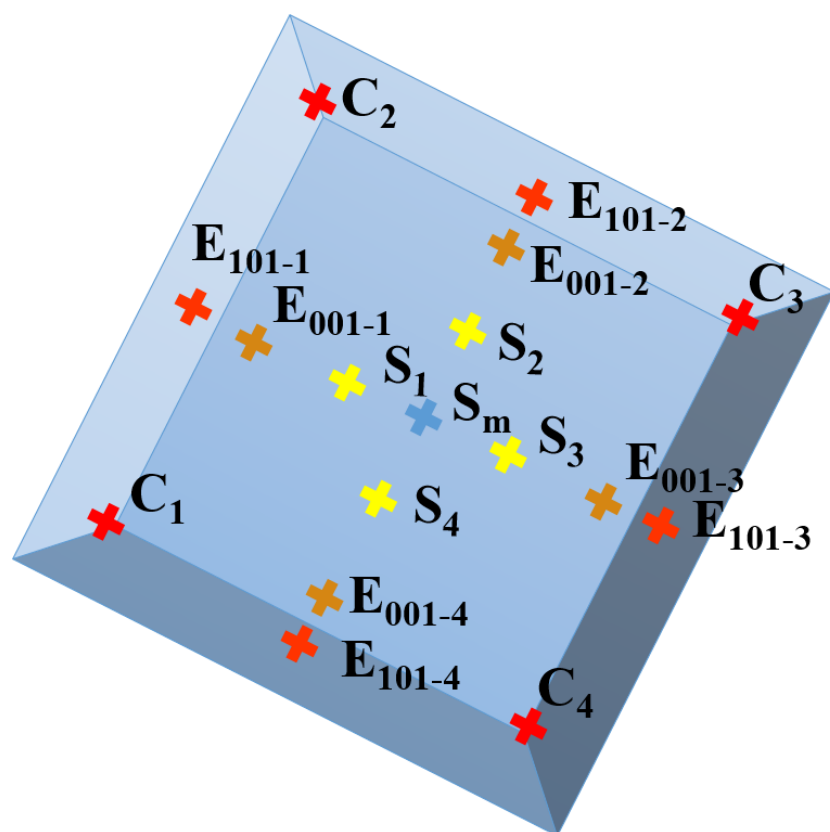


Fig. S4. Scheme showing several sites of a single anatase TiO₂ particle: surface S₁-S₄, edge E₀₀₁₋₁-E₀₀₁₋₄, edge E₁₀₁₋₁-E₁₀₁₋₄, and corner C₁-C₄.

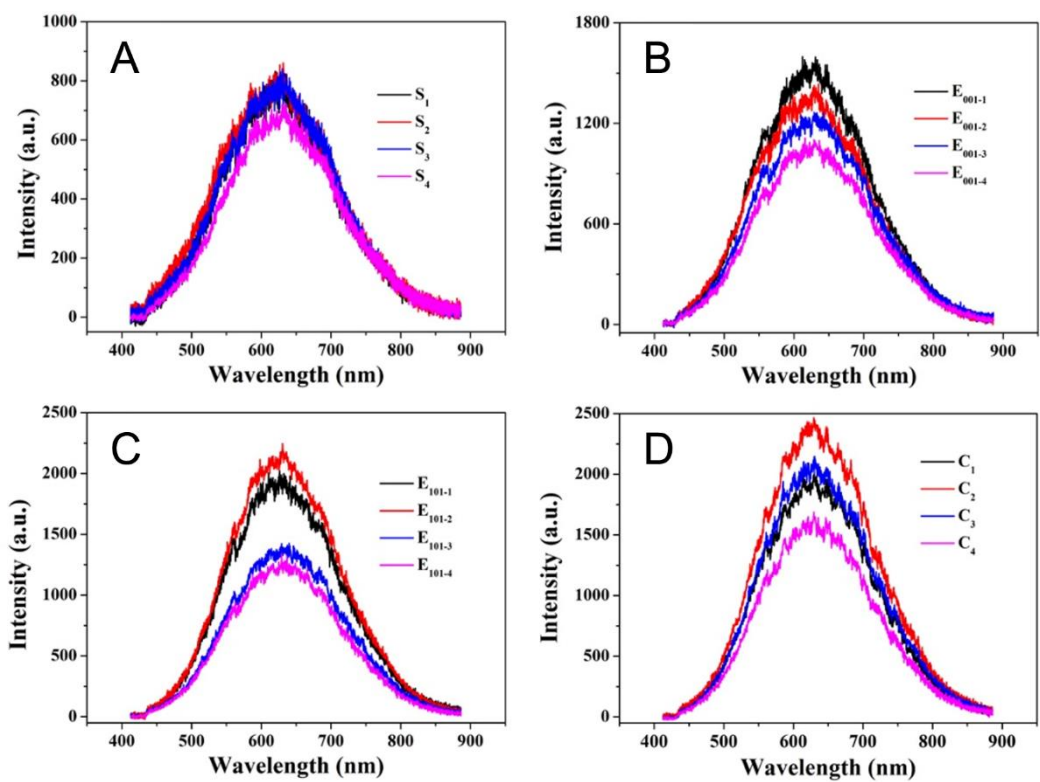


Fig. S5. PL spectra at several sites on a single anatase TiO₂ particle: (A) surface S₁-S₄, (B) edge E₀₀₁₋₁-E₀₀₁₋₄, (C) edge E₁₀₁₋₁-E₁₀₁₋₄, and (D) corner C₁-C₄.

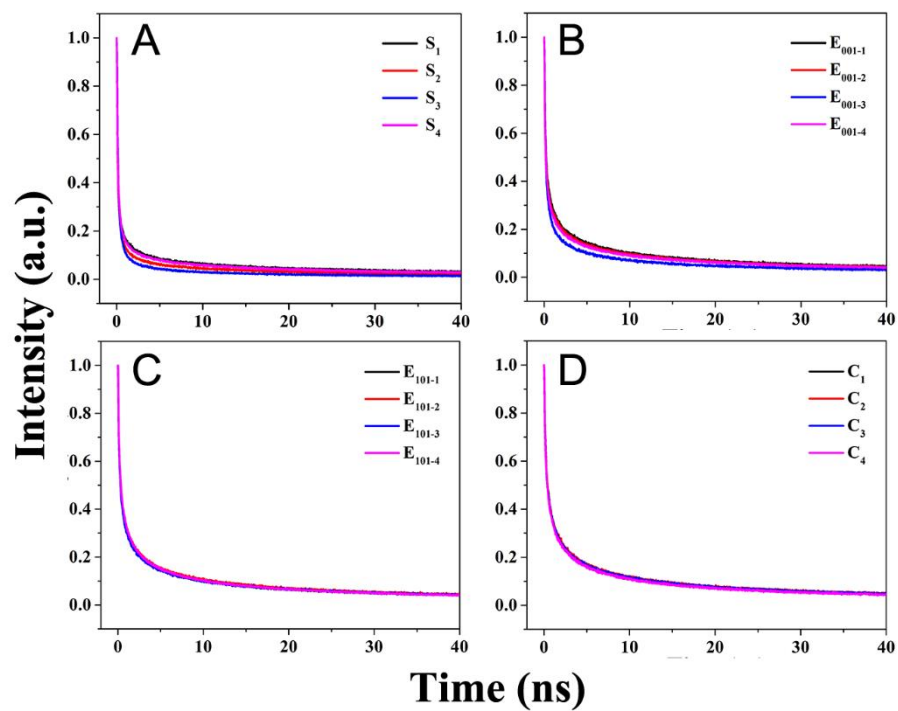


Fig. S6. PL decay profiles observed at several sites of a single anatase TiO₂ particle: (A) surface S₁-S₄, (B) edge E₀₀₁₋₁-E₀₀₁₋₄, (C) edge E₁₀₁₋₁-E₁₀₁₋₄, and (D) corner C₁-C₄.

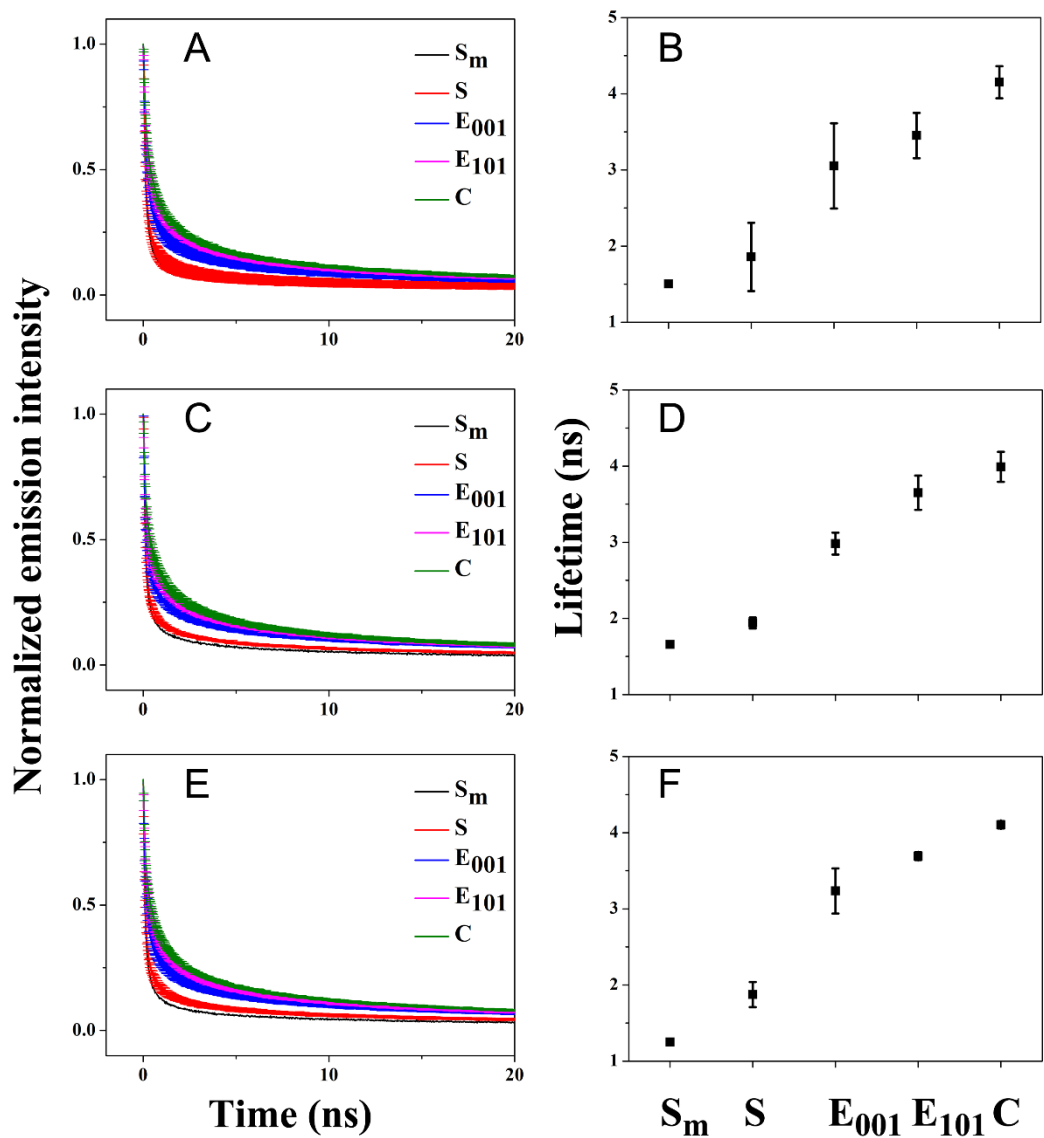


Fig. S7. Emission decay profiles and intensity-weighted emission lifetimes measured with error bars at various areas from the middle (S_m), S, E_{001} , and E_{101} to the corner (C) of an anatase TiO₂ particle. (A, B) for the particle in Fig. 2A, (C, D) for the particle in Fig. 3A, (E, F) for the particle in Fig. 3D.

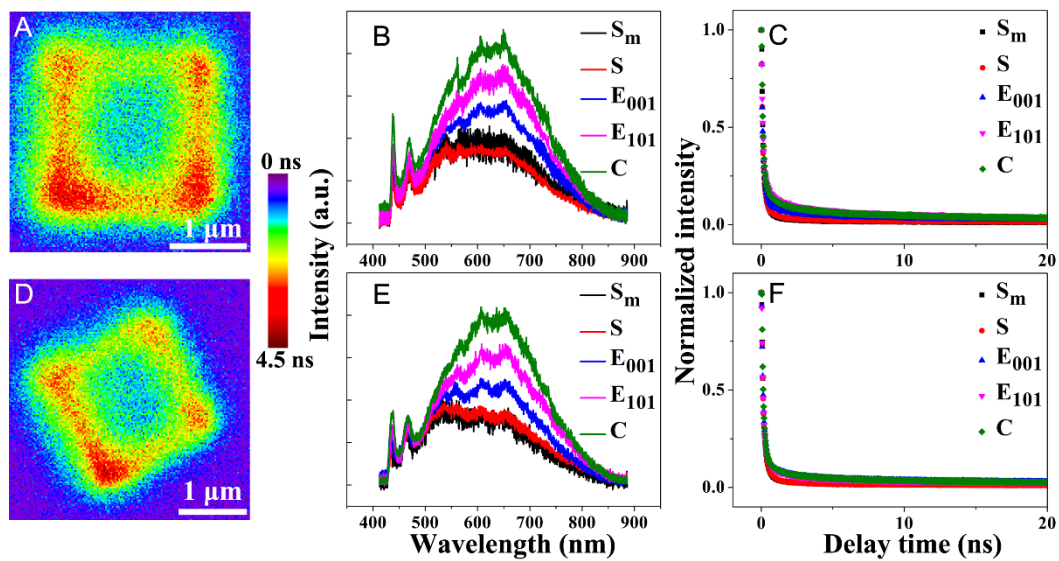


Fig. S8. (A, D) PL lifetime images of a single anatase TiO₂ particle ($\lambda_{\text{ex}} = 405$ nm, a femtosecond pulsed laser) (intensity bar: 0-4.5 ns); (B, E) the corresponding PL spectra at several sites; (C, F) the corresponding PL decay profiles from the middle site to the corner site for a single anatase TiO₂ particle.

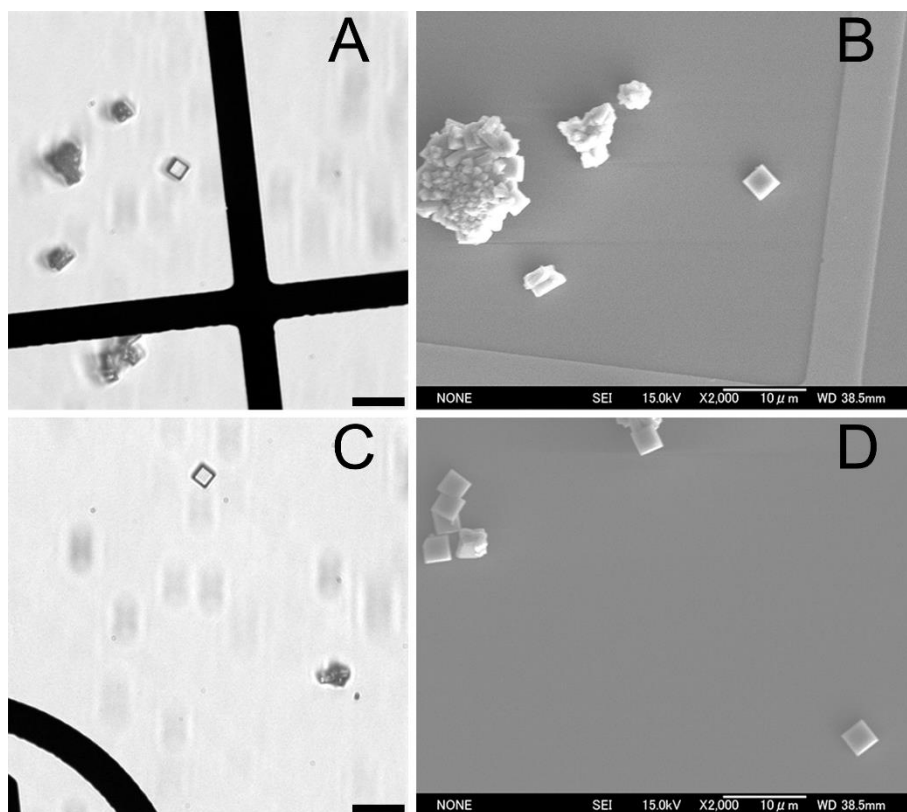


Fig. S9. (A, C) Phase-contrast microscope images (scale bar: 10 μm); (B, D) high-resolution SEM images for a single anatase TiO_2 particle for the measurement of PL decay profiles as shown in **Fig. S5**.

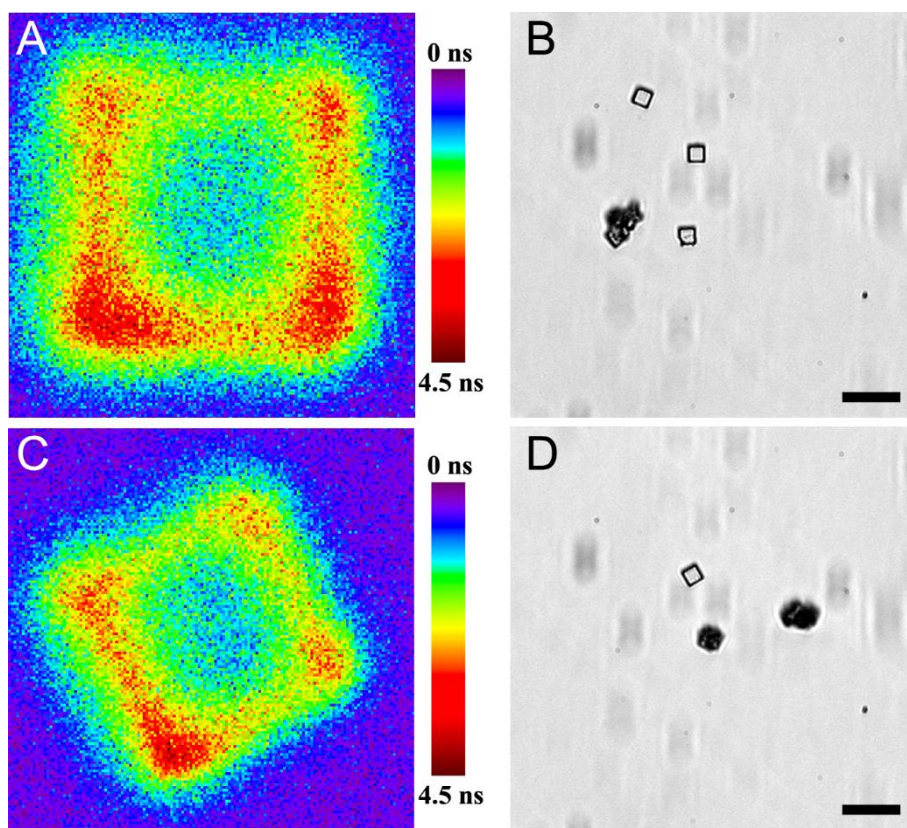


Fig. S10. PL (A, C) lifetime images of a single anatase TiO₂ particle ($\lambda_{\text{ex}} = 405$ nm, a femtosecond pulsed laser) (Intensity bar: 0-4.5 ns); (B, D) phase-contrast microscope images (scale bar: 10 μm).

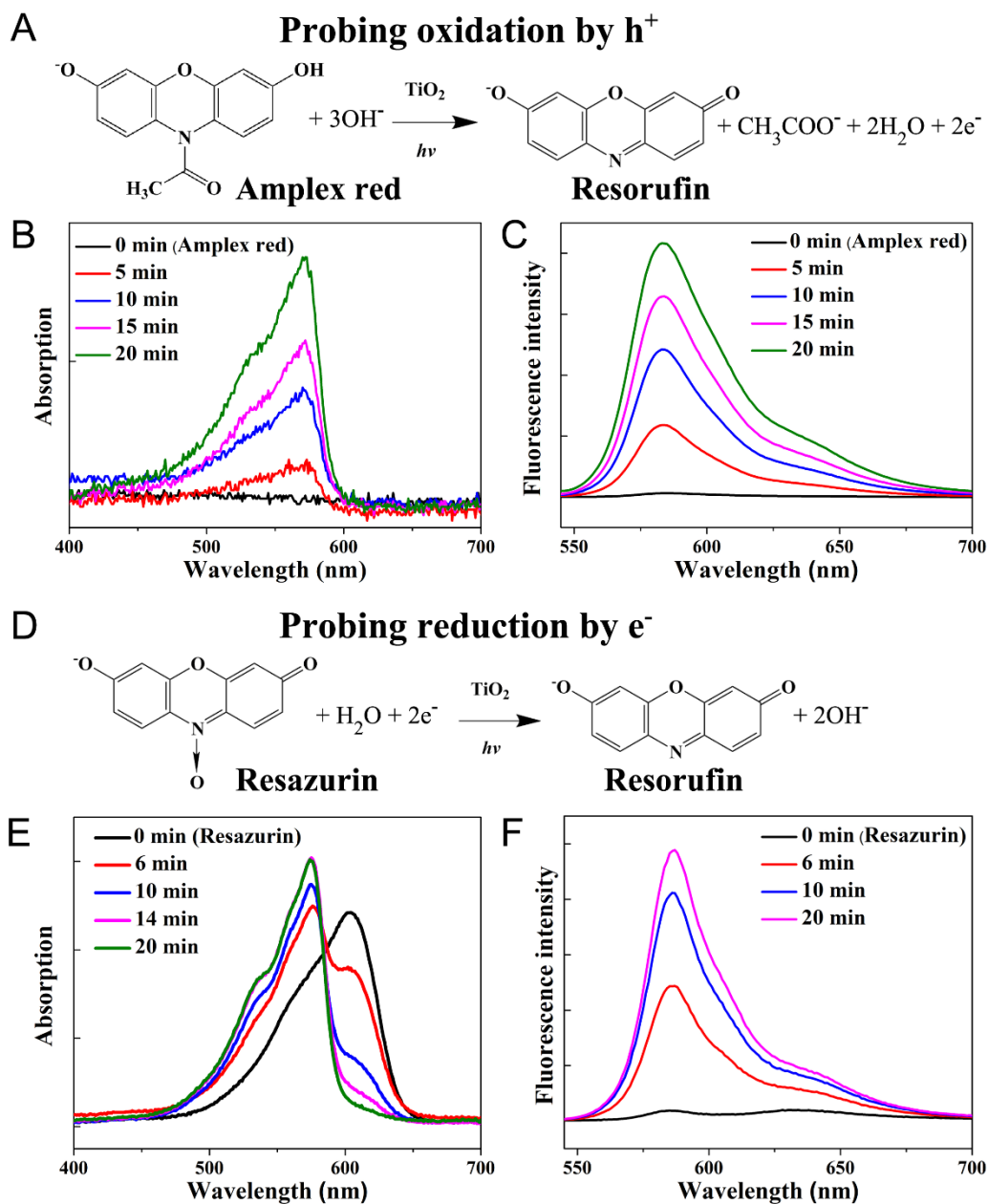


Fig. S11. Fluorogenic probe reactions: (A) oxidation of amplex red, (D) reduction of resazurin under UV irradiation of TiO_2 aqueous suspension. Absorption spectral changes in the oxidation (B) and reduction (E). Fluorescence spectral changes in the oxidation (C) and reduction (F). $\lambda_{\text{ex}} = 532 \text{ nm}$.

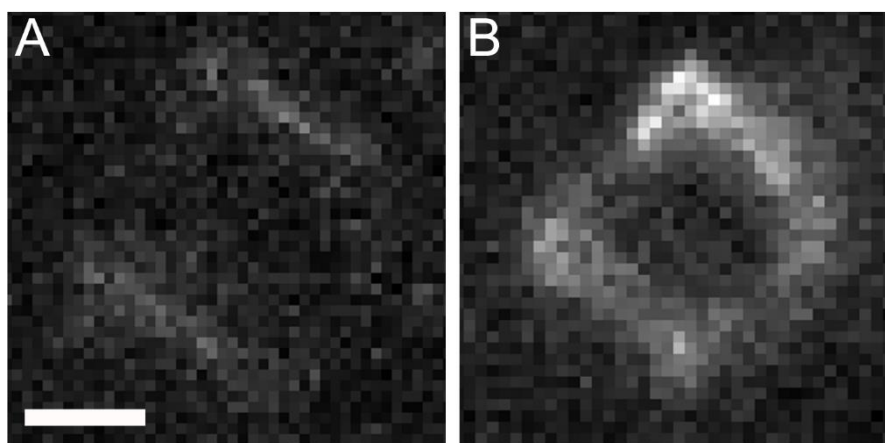
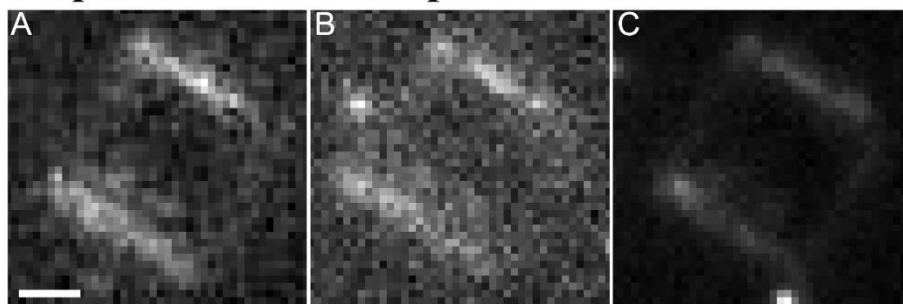


Fig. S12. Single-molecule fluorescence images on a single TiO_2 particle for the photocatalytic oxidation of amplex red (A) and reduction of resazurin (B) (scale bar: 1 μm).

Amplex red: oxidation probe of h^+



Resazurin: reduction probe of e^-

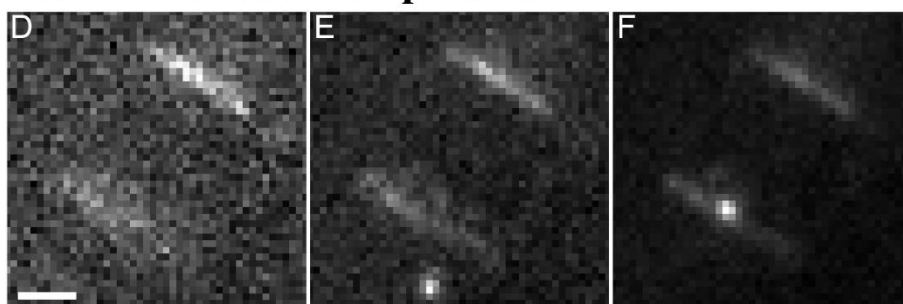


Fig. S13. Single-molecule fluorescence images on a single TiO_2 particle for the photocatalytic oxidation of amplex red at times of 0 (A), 4.5 (B), and 48.0 s (C) and the photocatalytic reduction of resazurin at times of 0 (D), 18.5 (E), and 52.8 s (F). Scale bar, 1 μm .

Supplementary Tables

Table S1. PL lifetimes at several sites of anatase TiO₂ particles (**Fig. 2A**)

Sites	τ_1 (ns)	Ratio (%)	τ_2 (ns)	Ratio (%)	τ_3 (ns)	Ratio (%)
S _m	0.14	82	1.71	13	23.3	5
S ₁	0.11	74	1.59	18	22.8	7
E ₀₀₁₋₁	0.14	64	2.09	24	23.9	12
E ₁₀₁₋₁	0.18	62	2.23	26	23.3	12
S ₂	0.13	74	1.91	18	24.2	8
E ₀₀₁₋₂	0.15	66	2.19	23	24.5	11
E ₁₀₁₋₂	0.16	61	2.12	27	23.0	12
S ₃	0.15	78	1.76	15	23.6	6
E ₀₀₁₋₃	0.15	68	2.16	22	24.1	11
E ₁₀₁₋₃	0.17	58	2.25	29	23.5	13
S ₄	0.13	77	1.21	18	19.5	5
E ₀₀₁₋₄	0.14	72	1.71	20	22.3	8
E ₁₀₁₋₄	0.16	64	2.02	25	22.5	11
C ₁	0.18	56	2.23	31	22.8	14
C ₂	0.20	56	2.33	30	23.7	14
C ₃	0.21	54	2.41	32	23.8	15
C ₄	0.18	55	2.26	30	23.3	14

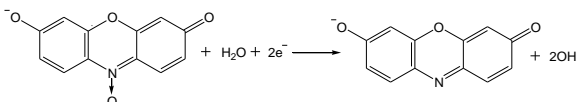
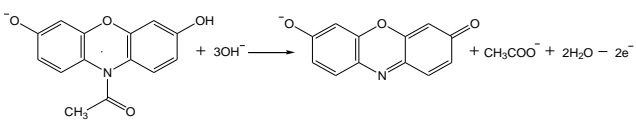
Table S2. PL lifetimes at several sites of anatase TiO₂ particles (**Fig. 3A**)

Sites	τ_1 (ns)	Ratio (%)	τ_2 (ns)	Ratio (%)	τ_3 (ns)	Ratio (%)
S _m	0.12	81	1.61	13	22.5	6
S ₁	0.12	79	1.82	14	23.5	7
E ₀₀₁₋₁	0.14	69	2.08	21	23.5	10
E ₁₀₁₋₁	0.15	58	2.06	29	21.7	13
S ₂	0.12	79	1.81	14	22.9	7
E ₀₀₁₋₂	0.12	62	1.88	26	21.8	12
E ₁₀₁₋₂	0.15	56	2.05	30	21.3	14
S ₃	0.12	79	1.79	14	23.3	7
E ₀₀₁₋₃	0.15	68	2.11	22	23.0	10
E ₁₀₁₋₃	0.15	56	2.07	29	21.8	15
S ₄	0.13	81	1.91	13	24.7	6
E ₀₀₁₋₄	0.12	66	1.89	23	22.6	11
E ₁₀₁₋₄	0.14	59	2.03	28	21.6	13
C ₁	0.19	55	2.26	31	22.0	14
C ₂	0.18	56	2.14	30	21.6	14
C ₃	0.20	54	2.27	31	22.1	15
C ₄	0.20	55	2.37	30	22.4	15

Table S3. PL lifetimes at several sites of anatase TiO₂ particles (**Fig. 3D**)

Sites	τ_1 (ns)	Ratio (%)	τ_2 (ns)	Ratio (%)	τ_3 (ns)	Ratio (%)
S _m	0.10	80	1.17	15	19.9	5
S ₁	0.10	77	1.50	16	21.8	7
E ₀₀₁₋₁	0.13	64	2.06	24	22.5	12
E ₁₀₁₋₁	0.18	55	2.16	31	21.1	14
S ₂	0.10	74	1.57	18	21.1	8
E ₀₀₁₋₂	0.14	59	2.01	28	21.3	13
E ₁₀₁₋₂	0.18	56	2.18	30	21.4	14
S ₃	0.10	73	1.37	19	20.2	8
E ₀₀₁₋₃	0.15	58	1.98	29	21.4	13
E ₁₀₁₋₃	0.16	55	2.00	31	21.0	14
S ₄	0.10	72	1.12	21	19.3	7
E ₀₀₁₋₄	0.11	65	1.62	24	21.3	11
E ₁₀₁₋₄	0.17	56	2.09	30	20.9	14
C ₁	0.19	53	2.22	32	21.5	15
C ₂	0.20	53	2.27	32	22.1	15
C ₃	0.21	53	2.24	32	21.9	15
C ₄	0.21	54	2.33	31	21.9	15

Table S4. Calculated thermodynamic (Gibb's free energy change, ΔG) and kinetic properties (energy barrier, E_a) of the fluorogenic probe reactions on anatase TiO_2 (001) surface and (101) surface, and their crystal edge.

Reactions	Reaction sites	ΔG (eV)	E_a (eV)
	(101) surface	-0.263	4.66
	Crystal edge	-0.657	2.82
	(001) surface	-1.10	3.54
	Crystal edge	-1.60	-0.22*

*The negative activation energy represents the barrierless reaction with a high reaction rate by capturing the molecules in a potential well.

Supplementary References

- (1) Ni, B.; Wang, X. Face the edges: Catalytic active sites of nanomaterials. *Adv Sci* **2015**, *2*, 1500085.
- (2) Rex, R. E.; Knorr, F. J.; McHale, J. L. Imaging luminescent traps on single anatase TiO₂ crystals: The influence of surface capping on photoluminescence and charge transport. *J. Phys. Chem. C* **2015**, *119*, 26212-26218.
- (3) Oprea, C. I.; Girtu, M. A. Structure and electronic properties of TiO₂ nanoclusters and dye-nanocluster systems appropriate to model hybrid photovoltaic or photocatalytic applications. *Nanomaterials-Basel* **2019**, *9*, 357.
- (4) Xia, Y. N.; Xiong, Y. J.; Lim, B.; Skrabalak, S. E. Shape-controlled synthesis of metal nanocrystals: Simple chemistry meets complex physics? *Angew. Chem. Int. Ed.* **2009**, *48*, 60-103.
- (5) Kottmann, J. P.; Martin, O. J. F.; Smith, D. R.; Schultz, S. Plasmon resonances of silver nanowires with a nonregular cross section. *Phys. Rev. B* **2001**, *64*, 235402.
- (6) Zhang, A. Y.; Wang, W. Y.; Chen, J. J.; Liu, C.; Li, Q. X.; Zhang, X.; Li, W. W.; Si, Y.; Yu, H. Q. Epitaxial facet junctions on TiO₂ single crystals for efficient photocatalytic water splitting. *Energy Environ. Sci.* **2018**, *11*, 1444-1448.
- (7) Hussain, A. A computational study of catalysis by gold in applications of CO oxidation. Ph.D. Thesis. Technische Universiteit Eindhoven, 2010.
- (8) Toroker, M. C.; Kanan, D. K.; Alidoust, N.; Isseroff, L. Y.; Liao, P. L.; Carter, E. A. First principles scheme to evaluate band edge positions in potential transition metal oxide photocatalysts and photoelectrodes. *Phys. Chem. Chem. Phys.* **2011**, *13*, 16644-16654.
- (9) Greiner, M. T.; Helander, M. G.; Tang, W.-M.; Wang, Z.-B.; Qiu, J.; Lu, Z.-H. Universal energy-level alignment of molecules on metal oxides. *Nat. Mater.* **2011**, *11*, 76-81.
- (10) Li, Y.; Liu, Z.; Liu, L.; Gao, W. Mechanism and activity of photocatalytic oxygen evolution on titania anatase in aqueous surroundings. *J. Am. Chem. Soc.* **2010**, *132*, 13008-13015.
- (11) Valdés, A.; Qu, Z. W.; Kroes, G. J.; Rossmeisl, J.; Nørskov, J. K. Oxidation and photo-oxidation of water on TiO₂ surface. *J. Phys. Chem. C* **2008**, *112*, 9872-9879.